# High-Performance Control of Doubly-Fed Reluctance Machines

Milutin Jovanović and Hamza Chaal

*Abstract*—**The Brushless Doubly Fed Reluctance Machine (BDFRM) is a promising cost-effective alternative solution in applications with narrow speed ranges such as large wind turbines and/or pump-type drives. Apart from providing a comprehensive literature review and analysis of vector (field-oriented) control and direct torque (and flux) control (DTC) methods, the development, and results of experimental verification, of an angular velocity observer-based DTC scheme for sensorless speed operation of the BDFRM which, unlike most of the other DTC concepts, can perform well down to zero supply frequency of the inverter-fed winding, have also been presented in the paper.**

*Index Terms*—**Control, brushless doubly fed reluctance machines, slip power recovery systems, wind turbines.**

## I. Introduction

ALTHOUGH the inverter-fed brushless doubly fed reluctance machine (BDFRM) has not found any industrial use yet, it is an attractive low cost candidate for variable speed applications due to the high reliability and lower harmonic injection into the mains. The economic benefits [1] come from its slip power recovery property which allows the use of a smaller inverter (relative to the machine rating), and especially if the speed range required is limited (e.g. in large wind turbines or pumps [2, 3]). The BDFRM has two standard, sinusoidally distributed stator windings of different applied frequencies and pole numbers - the primary (or power) winding is with direct on-line supply and the secondary (or control) winding is also grid-connected but through a bi-directional (back-to-back) converter. In order to provide rotor position dependent magnetic coupling between the windings and torque production from the machine [4, 5], the reluctance rotor must have half the total number of stator poles. Such an unusual operating principle [6] implies the modest torque per volume of the BDFRM compared to an equivalent synchronous reluctance or induction machine [7]. The BDFRM shares all the advantages of doubly-fed machines over singly excited cousins – the operational mode flexibility, the greater control freedom, and the wider speed ranges i.e. the possibility of subsynchronous and super-synchronous operation in both motoring and generating regimes [7]. It can work as a conventional induction machine (which is an important "fail-safe" measure in case of the inverter failure) or as a fixed/adjustable speed synchronous turbo-machine [8]. One important BDFRM merit is that one can not only control torque, but also the power factor [3, 9–11], efficiency [2] or any other performance parameter of interest in an inherently decoupled fashion [12].

M. Jovanović and H. Chaal are with Northumbria University, Newcastle upon Tyne NE1 8ST, United Kingdom (e-mail: milutin.jovanovic@northumbria.ac.uk).

The absence of brush gear brings a clear advantage to the BDFRM over a conventional doubly-excited wound rotor induction machine (DEWRIM) in applications where increased reliability and lower maintenance are crucial factors (for example, off-shore wind generators). Furthermore, the BDFRM is more efficient [13] and easier to control than the closely related, brushless doubly-fed induction machine (BDFIM) having the same stator as the BDFRM but with a special cage rotor [14–17]. Recent FEA studies have shown that with higher rotor saliency-ratios, the BDFRM overall performance can be improved [7] to a level competitive with the induction machine [18]. The primary intention of this paper is to review control methodologies reported in the BDFRM literature. By integrating the existing knowledge, this survey may serve as a useful up-to-date reference for future research on this machine. Algorithms for scalar control, direct torque (and flux) control (DTC) and field-oriented control have already been proposed and evaluated by simulations [2, 19] and experimentally [12, 20]. However, these approaches all rely on using an encoder for rotor position and/or speed detection. Eliminating a shaft position sensor would not only reduce the system cost but, more importantly, would further enhance its reliability. The theoretical considerations in [21] and [22] have concerned with sensorless vector control and DTC, respectively. The simulation studies carried out in [11, 22] have been practically validated in [3, 10, 11]. This paper will reproduce the major outcomes of this experimental work.

## II. Dynamic Modeling

The space-vector equations for the BDFRM in a stationary reference frame using standard notation and motoring convention are [4, 6, 23]:

$$\underline{u}_{p_s} = R_p \underline{i}_{p_s} + \frac{d\underline{\lambda}_{p_s}}{dt} = R_p \underline{i}_{p_s} + \left.\frac{d\underline{\lambda}_{p_s}}{dt}\right|_{\theta_p \text{const}} + j\omega_s \underline{\lambda}_{p_s} \quad (1)$$

$$\underline{u}_{s_s} = R_s \underline{i}_{s_s} + \frac{d\underline{\lambda}_{s_s}}{dt} = R_s \underline{i}_{s_s} + \left.\frac{d\underline{\lambda}_{s_s}}{dt}\right|_{\theta_s \text{const}} + j\omega_s \underline{\lambda}_{s_s} \tag{2}$$

$$\underline{\lambda}_{p_s} = L_p \underline{i}_{p_s} + L_{ps} \underline{i}^*_{s_s} e^{j\theta_r} \tag{3}$$

$$\underline{\lambda}_{s_s} = L_s \underline{i}_{s_s} + L_{ps} \underline{i}^*_{p_s} e^{j\theta_r}\ . \tag{4}$$

The subscripts 'p' and 's' denote the primary and secondary winding quantities respectively, and '*' represents the complex conjugate. By omitting the exponential terms in (3)-(4), one obtains the rotating frame equivalents of (1)-(4) in a primary flux oriented form ($\lambda_{pq}= 0$):

$$\underline{u}_p = R_p \underline{i}_p + \frac{d\lambda_p}{dt} + j\omega_p \lambda_p \tag{5}$$

$$\underline{u}_s = R_s \underline{i}_s + \frac{d\underline{\lambda}_s}{dt} + j\omega_s \underline{\lambda}_s \tag{6}$$

$$\lambda_p = L_p \underline{i}_p + L_{ps} \underline{i}^*_s \tag{7}$$

$$\underline{\lambda}_s = L_s \underline{i}_s + L_{ps} \underline{i}^*_p = \sigma L_s \underline{i}_s + \underbrace{\frac{L_{ps}}{L_p}\lambda_p}_{\lambda_{ps}} \tag{8}$$

where $\sigma = 1 - L_{ps}^2/(L_pL_s) = 1 - k_{ps}^2$ is the leakage factor (defined as with the induction machine), $k_{ps} = L_{ps}=\sqrt{L_pL_s}$ is the coupling coefficient between the windings (as in the power transformer case), $L_{p;s;ps}$ are the respective 3-phase inductances [4, 7], and $\lambda_{ps}$ is the primary flux linking the secondary winding (Fig. 1).

Applying the fundamental BDFRM theory [4, 6, 23], the following condition for the machine torque production can be established:

$$\omega_r = p_r\omega_{rm} = \omega_p + \omega_s \Leftrightarrow \theta_r = p_r\theta_{rm} = \theta_p + \theta_s \tag{9}$$

where $\omega_{rm} = d\theta_{rm}/dt$ is the rotor mechanical angular velocity (rad/s), $p_r$ is the number of rotor poles, $\omega_{p,s} = d\theta_{p,s}/dt$ *are* the applied angular frequencies (rad/s) to the windings, and $\theta_{r,p,s}$ are the angular positions of the ro-tating reference frames as illustrated in Fig. 1 (the rotor frame is omitted for convenience). Notice that $\omega_s > 0$ for 'super-synchronous' $(\omega_{rm} > \omega_{syn})$ and $\omega_s < 0$ for 'subsynchronous' $(\omega_{rm} < \omega_{syn})$ machine operation where $\omega_{syn}= \omega_p/p_r$ occurs with the DC secondary winding i.e. when $\omega_s=0$. The 'negative' secondary frequency at sub-synchronous speeds simply means the opposite phase sequence of the secondary to the primary winding.

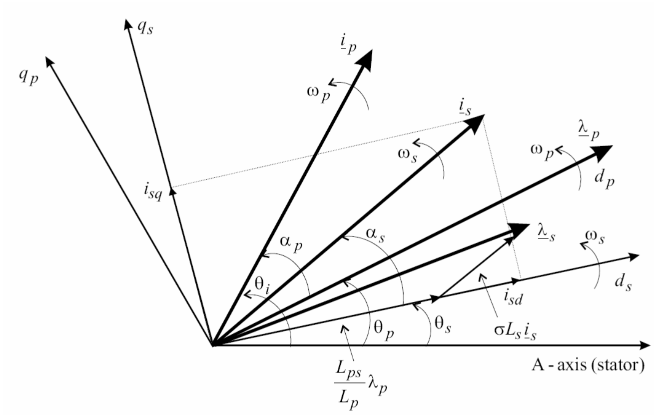


Fig. 1. Reference frames and characteristic phasors.

## III. Vector Control

The secondary real power, torque and primary reactive power in a primary flux oriented form are [4]:

$$P_s = \frac{\omega_s}{\omega_p + \omega_s} P_{out} = \frac{\omega_s}{\omega_p} P_p \tag{10}$$

$$T_e = \frac{P_{out}}{\omega_{rm}} = \frac{3}{2} p_r \frac{L_{ps}}{L_p} \lambda_p i_{sq} \tag{11}$$

$$Q_p = \frac{3}{2} \frac{\omega_p \lambda_p}{L_p} (\lambda_p - L_{ps} i_{sd})\ . \tag{12}$$

As can be seen from (11) and (12), Te is controlled by the secondary q-axis current, $i_{sq}$, and $Q_p$ by the secondary d-axis current, $i_{sd}$, and there is no coupling between the two expressions (since $\lambda_p$ is virtually constant). Note that the machine slip power recovery property is hidden in (10). For example, if the secondary is at the line frequency (i.e. $\omega_s = \omega_p$), the inverter has to handle half the output power (plus losses). However, if $\omega_s = 0.25\omega_p$, then the secondary contribution to the machine power production is only 20%. Therefore, in applications where the BDFRM would operate in a narrow range around the synchronous speed, a partially-rated inverter could do.

The structure of a typical BDFRM drive with vector control based on (11) and (12) is shown in Fig. 2 [12]. Considering that only the secondary winding quantities are controllable, one should first identify the secondary frame position ($\theta_s$) using (9). The rotor position, $\theta_{rm}$, is usually detected by a shaft sensor while the primary flux angle (Fig. 1), $\theta_p$, follows from:

$$\underline{\lambda}_{p_s} = \lambda_p e^{j\theta_p} = \int (\underline{u}_{p_s} - R_p \underline{i}_{p_s})dt \approx \int \underline{u}_{p_s} dt \tag{13}$$

where $\underline{u}_{ps}$ and $\underline{i}_{ps}$ can be easily determined from phase measurements. Once $\theta_s$ is known one can implement current control of the secondary $d_sq_s$ components (and thus $T_e$ and $Q_p$) in a traditional manner (Fig. 2) to optimise the desired performance parameter of the machine such as [2]: (1) the maximum torque per secondary (inverter) ampere (i.e. $i_{sd} = 0$) [7, 9]; (2) the maximum primary power factor (i.e. $i_{sd} = \lambda_p/L_{ps}$ for $Q_p = 0$) [9, 12]; (3) the unity line power factor or the minimum copper losses [9]; (4) the maximum power point tracking (MPPT) of a wind turbine [2] etc.

## IV. Direct Torque Control (DTC)

The traditional DTC concept, originally developed for cage induction machines [24, 25], by virtue of its versatility and fewer machine parameter dependence, has been successfully used for stator frame control of almost all brushless machines. However, until very recently, its application to doubly-fed machines (DFMs) in general has been little reported in the literature. An alternative rotor frame based DTC technique for the BDFIM required a shaft position sensor for torque control,

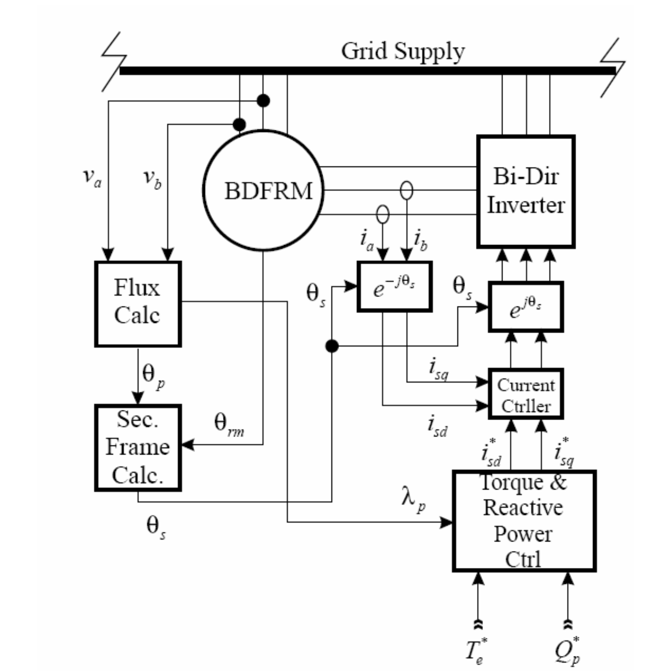


Fig. 2. A simplified block diagram of the field-oriented torque controller for the BDFRM.

and it was very complex even for DSP implementation [26]. The DTC schemes presented in [27–29] for a conventional doubly-fed induction generator (DFIG), on the other hand, have only been studied by computer simulations. In the last couple of years, predictive DTC strategies of constant switching frequency have been proposed and experimentally verified for the DEWRIM but used an encoder for control purposes [30–32]. Except for the recent practical work on the BDFRM control [10, 11], the only other test validation of sensorless DTC for DFMs has appeared in [33]. While a viable, parameter-independent algorithm for unity power factor control of the DFIG has been developed, the sustained synchronous speed operation of the machine has not been clearly demonstrated.

It is well-known that back-emf based control approaches, including DTC, have low frequency stability problems due to the flux estimation inaccuracies caused by resistance variations at lower supply voltages. It is mainly for this reason that this control method has been extremely popular for high-speed applications where the resistance effects are less pronounced. In this respect, the traditional DTC is not suitable for BDFRM applications. Fortunately, these common DTC difficulties at low secondary frequencies can be overcome in the BDFRM.

### *A. Main Principles*

One of the key questions of the DTC of the BDFRM, as for any other machine, is how to control the secondary flux to achieve the desired torque dynamics. An answer can be found in (8) and a DTC form of (11):

$$\underline{\lambda}_s = \lambda_{sd} + j\lambda_{sq} = \sigma L_s i_{sd} + \lambda_{ps} + j\sigma L_s i_{sq} \tag{14}$$

$$T_e = \frac{3p_r}{2\sigma L_s}\left|\underline{\lambda}_{ps} \times \underline{\lambda}_s\right| = \frac{3p_r}{2\sigma L_s}\underbrace{\frac{L_{ps}}{L_p}\lambda_p}_{\lambda_{ps}}\lambda_s \sin\delta\,. \tag{15}$$

It is evident from (14) and (11) that $\lambda_{sq}$ is a torque producing secondary flux component since it is directly proportional to $i_{sq}$. Therefore, in order to increase (decrease) instantaneous torque for a given $\lambda_s$, one needs to apply appropriate voltage vectors to the secondary winding to allow the secondary flux angle in the $d_sq_s$ frame (Fig. 1), i.e. $\delta$ in (15), to increase (decrease). This effectively means that the respective stationary frame angle, $\delta + \theta_s$, would also change accordingly as $\theta_s$ variations are negligible (and especially at low $\omega_s$ values) over a short control interval dictated by the inherently high sampling rates. There is obviously no need to know the secondary frame position, and the DTC can be implemented in a stator frame as usual for this method.

The outputs of the flux and torque comparators in the DTC algorithm (Fig. 3) can be defined as:

$$\Delta\lambda_s = \begin{cases} 1, & \lambda_s^* - \lambda_s \ge \Delta\lambda \\ 0, & \lambda_s^* - \lambda_s \le -\Delta\lambda \end{cases} \tag{16}$$

$$\Delta T_e = \begin{cases} 1, & T_e^* - T_e \ge \Delta T \\ -1, & T_e^* - T_e \le -\Delta T \end{cases} \tag{17}$$

where $\Delta T$ and $\Delta\lambda$ indicate a half width of the corresponding hysteresis bands. The voltage vectors generated by the inverter to achieve the desired control action for a particular sectorial location of the secondary flux vector are given in Table I. The

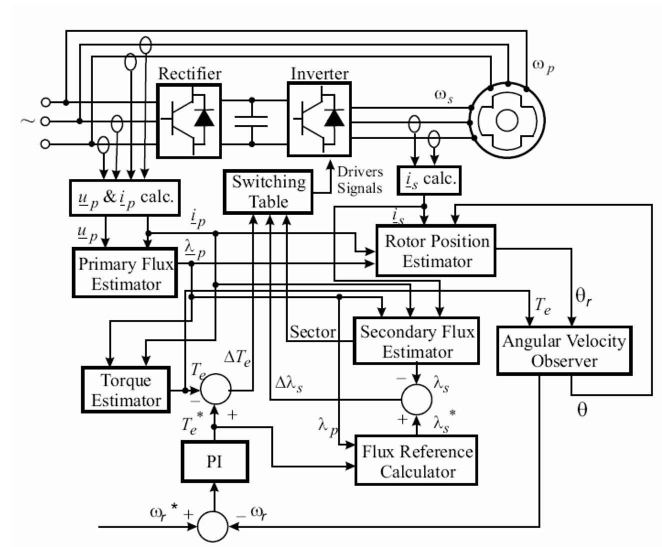


Fig. 3. Sensorless BDFRM drive with DTC.

TABLE I
INVERTER SWITCHING LOOK-UP TABLE

| Comparator | | Secondary Flux Sector | | | | | |
|---|---|---|---|---|---|---|---|
| $\Delta\lambda_S$ | $\Delta T_e$ | 1 | 2 | 3 | 4 | 5 | 6 |
| 1 | 1 | $U_2$ | $U_3$ | $U_4$ | $U_5$ | $U_6$ | $U_1$ |
| 1 | -1 | $U_6$ | $U_1$ | $U_2$ | $U_3$ | $U_4$ | $U_5$ |
| 0 | 1 | $U_3$ | $U_4$ | $U_5$ | $U_6$ | $U_1$ | $U_2$ |
| 0 | -1 | $U_5$ | $U_6$ | $U_1$ | $U_2$ | $U_3$ | $U_4$ |

respective magnitudes and angular positions in a stationary frame can be expressed as follows:

$$\underline{U}_k = \frac{2}{3} V_{dc} e^{j(k-1)\frac{\pi}{3}} \quad k = 1, 2, ..., 6 \tag{18}$$

where $V_{dc}$ is the measured DC link voltage and $[(2k - 3)\pi/6; (2k-1)\pi/6]$ are the angular boundaries of the k-th sector associated with $\underline{U}_k$. The binary codes, indicating the switching status of individual inverter legs of these vectors are: $\underline{U}_1$ = 100, $\underline{U}_2$ = 110, $\underline{U}_3$ = 010, $\underline{U}_4$ = 011, $\underline{U}_5$ = 001, and $\underline{U}_6$ = 101.

The controller's main task is to ensure that the secondary flux and machine torque are kept within the userspecified hysteresis bands. In the flux case, according to (16), the $\lambda_s$ values should be in the range $[\lambda_s^* - \Delta\lambda$ ¸ $\lambda_s^* + \Delta\lambda]$ with $\Delta\lambda_s = 1$ voltage vectors increasing, and $\Delta\lambda_s = 0$ vectors decreasing the $\lambda_s$ magnitudes (Table I). Similarly in (17), $\Delta T_e = 1$ means the increase, and $\Delta T_e = -1$ the decrease of actual (not absolute) torque which is assumed positive if acting counter-clockwise as in Fig. 1. Note that the influence of zero voltage vectors ($\underline{U}_0$ = 000 and $\underline{U}_7$ = 111) on torque behavior is speed dependent (refer to [19, 22] for further details). For this reason, the switching strategy adopted is based on using the active voltage vectors only and knowledge of the machine speed for torque control is not required (Fig. 3).

### *B. Parameter Estimation*

As discussed earlier, the use of (2) for estimating the secondary flux magnitude and stationary frame angle is not convenient in the low frequency region. However, as both the primary and secondary quantities are measurable, the following alternative expression can be derived using (1), (3) and (4):

$$\underline{\lambda}_{s_s} = L_s \underline{i}_{s_s} + \underline{i}_{p_s}^* \frac{\underline{\lambda}_{p_s} - L_p \underline{i}_{p_s}}{\underline{i}_{s_s}^*} \tag{19}$$

where $\lambda_{ps}$ is given by (13). The magnitudes and angular positions of $\underline{i}_{ss}$ and $\underline{i}_{ps}$ can be calculated from measurements [19, 20, 22]. Applying (19) one would obviously avoid the voltage integration but at the expense of having to know the winding self inductances $L_{p;s}$.

Another significant benefit of greater control freedom, afforded by the accessibility of both BDFRM windings, is the possibility of sensorless speed control [22]. The rotor angle, $\theta_r$, can be retrieved from (3) as follows:

$$\left.\begin{aligned} \theta_{r_1} &= \tan^{-1} \frac{\mathrm{Im}[(\underline{\lambda}_p - L_p \underline{i}_p)\underline{i}_s]}{\mathrm{Re}[(\underline{\lambda}_p - L_p \underline{i}_p)\underline{i}_s]} \\ \theta_{r_2} &= \theta_{r_1} + \pi \end{aligned}\right\} \tag{20}$$

The raw position estimates are then input to a Luenberger type PI observer to predict the rotor angular velocity $\omega_r = d\theta/dt$ for the speed control (Fig. 3).

The torque expression best suited for the BDFRM control is of the form:

$$T_e = \frac{3}{2} p_r \left| \underline{\lambda}_{p_s} \times \underline{i}_{p_s} \right| = \frac{3}{2} p_r (\lambda_{pd} i_{pq} - \lambda_{pq} i_{pd}) \tag{21}$$

where the subscripts '*pd*' and '*pq*' indicate the respective stator frame components (Fig. 1) of $\underline{\lambda}_{ps}$ and $\underline{i}_{ps}$. High estimation accuracy has been achieved in practice as (21) is nearly machine parameter independent (except for indirect $R_p$ effects through ¸$\lambda_p$ estimates) and relies on the primary 'ripple-free' quantities of fixed line frequency.

## V. Experimental Results

The sensorless control algorithm in Fig. 3 was executed in dSPACE® at 10 kHz on a small BDFRM prototype [19, 20]. The preliminary tests were conducted for the unloaded machine to assess the controller viability.

The plots in Fig. 4 represent the rotor angles ($\theta_r$) obtained from (20), and their absolute variations from encoder measurements. A shaft position sensor was used for monitoring purposes only and is not shown in Fig. 3. The raw estimates, $\theta_r$; are notably noisy, the error spikes being occasionally larger than 30º. Despite this, the average estimation error is reasonably low (≈ 7º).

The excellent low-pass filtering abilities of the observer are evident from Fig. 5. The average estimation error is reduced to approximately 1.5º with the maximum values being up to about 3.4º. Such accuracy improvement can be attributed to the high quality estimates being fed into the observer by the position estimator (Fig. 3). The observer last prediction, $\theta$, has served as a reference while selecting the best raw estimate available per speed control interval i.e. the one having the least absolute deviation from $\theta$. Therefore, the estimator block itself carries out the first filtering of noisy $\theta_r$ before inputting the best estimate to the observer for further processing. The filtered $\theta_r$ values are plotted out in Fig. 4.

Fig. 6 shows the machine response to a varying speed reference values between 950 rpm, 750 rpm and 550 rpm. The speed limits correspond to $fs \approx 13.3$ Hz in either super- or sub-synchronous mode. It can be seen that the machine can be

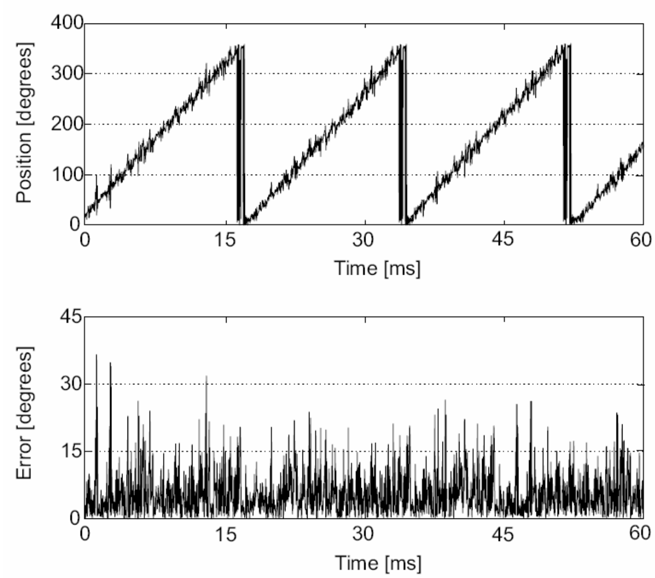


Fig. 4. Estimated position and estimator absolute errors at 850 rpm ($fs$ = 6.7 Hz).

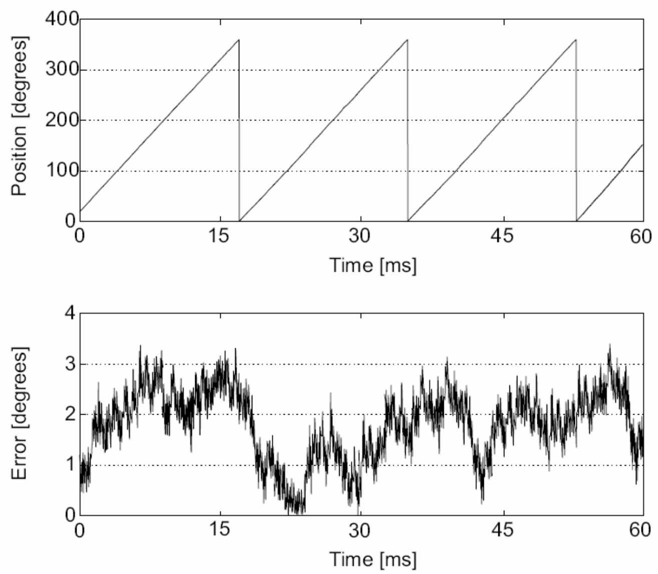


Fig. 5. Observed position and observer errors corresponding to Fig. 4.

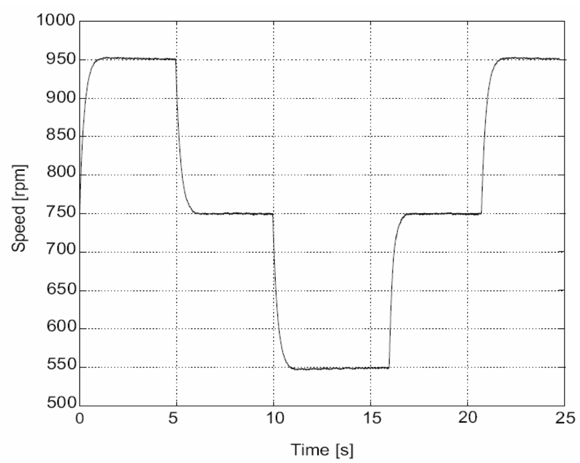


Fig. 6. Sensorless control performance down to synchronous speed.

effectively controlled over the considered speed range down to synchronous speed (750 rpm) when $f_s$ = 0. The reliable low frequency operation of the BDFRM is an important merit of the proposed sensorless scheme, and represents a significant advantage over traditional DTC and other back-emf based control methods having difficulties (or simply not working) in this frequency region even in sensor speed mode.

## VI. CONCLUSIONS

The fundamental principles and implementation aspects of different control techniques for the BDFRM have been surveyed in this paper. This kind of unified study can be extremely helpful for control development and research on this interesting and unusual slip-power recovery machine. A similar control related framework for the BDFRM or any other doubly fed machine has not been published in the refereed literature to date.

## REFERENCES

[1] Y. Liao, “Design of a brushless doubly-fed induction motor for adjustable speed drive applications,” *Proc. of the IEEE IAS Annual Meeting*, pp. 850–855, San Diego, California, October 1996.

[2] M.G.Jovanović, R.E.Betz, and J.Yu, “The use of doubly fed reluctance machines for large pumps and wind turbines,” *IEEE Transactions on Industry Applications*, vol. 38, no. 6, pp. 1508–1516, Nov/Dec 2002.

[3] D.G.Dorrell and M.Jovanovic, "On the possibilities of using a brushless doubly-fed reluctance generator in a 2 MW wind turbine," *IEEE Industry Applications Society Annual Meeting (IAS),* pp. 1-8, 5-9 October 2008.

[4] R.E.Betz and M.G.Jovanovic, "Introduction to the space vector modelling of the brushless doubly-fed reluctance machine," *Electric Power Components and Systems,* vol. 31, no. 8, pp. 729-755, August 2003.

[5] "Theoretical analysis of control properties for the brushless doubly fed reluctance machine," *IEEE Transactions on Energy Conversion,* vol. 17, no. 3, pp. 332-339, Sept 2002.

[6] Y. Liao, L. Xu, and L. Zhen, "Design of a doubly-fed reluctance motor for adjustable speed drives," *IEEE Transactions on Industry Applications,* vol. 32, pp. 1195-1203, Sept/Oct 1996.

[7] R.E.Betz and M.G.Jovanovic, "The brushless doubly fed reluctance machine and the synchronous reluctance machine - a comparison," *IEEE Transactions on Industry Applications,* vol. 36, no. 4, pp. 1103-1110, July/August 2000.

[8] O.Ojo and Z.Wu, "Synchronous operation of a dual-winding reluctance generator," *IEEE Transactions on Energy Conversion,* vol. 12, no. 4, pp. 357-362, December 1997.

[9] M.G.Jovanovic and R.E.Betz, "Power factor control using brushless doubly fed reluctance machines," *Proc. of the IEEE-IAS Annual Meeting,* vol. 1, pp. 523-530, Rome, Italy, October 2000.

[10] M.G.Jovanovic and M.M.R.Ahmed, "Sensorless speed control strategy for brushless doubly-fed reluctance machines," *Electric Machines and Drives Conference (IEMDC),* vol. 2, pp. 1514-1519, 3-5 May 2007.

[11] M.G.Jovanovic and D.G.Dorrell, "Sensorless control of brush less doubly-fed reluctance machines using an angular velocity observer," *Power Electronics and Drive Systems (PEDS),* pp. 717— 724, 27-30 November 2007.

[12] L. Xu, L. Zhen, and E. Kim, "Field-orientation control of a doubly excited brushless reluctance machine," *IEEE Transactions on Industry Applications,* vol. 34, no. 1, pp. 148-155, Jan/Feb 1998.

[13] F.Wang, F.Zhang, and L.Xu, "Parameter and performance comparison of doubly-fed brushless machine with cage and reluctance rotors," *IEEE Transactions on Industry Applications,* vol. 38, no. 5, pp. 1237-1243, Sept/Oct 2002.

[14] S. Williamson, A. Ferreira, and A. Wallace, "Generalised theory of the brushless doubly-fed machine. part 1: Analysis," *IEE Proc. -Electric Power Appl.,* vol. 144, no. 2, pp. 111-122, March 1997.

[15] P.C.Roberts, R.A.McMahon, P.J.Tavner, J.M.Maciejowski, and T.J.Flack, "Equivalent circuit for the brushless doubly fed machine (BDFM) including parameter estimation and experimental verification," *IEE Proc.-Electr. Power Appl.,* vol. 152, no. 4, pp. 933-942, July 2005.

[16] R.A.McMahon, P.C.Roberts, X.Wang, and P.J.Tavner, "Performance of BDFM as generator and motor," *IEE Proc.-Electr. Power Appl.,* vol. 153, no. 2, pp. 289-299, March 2006.

[17] J. Poza, E. Oyarbide, D. Roye, and M. Rodriguez, "Unified reference frame dq model of the brushless doubly fed machine," *IEE Proc.-Electr. Power Appl.,* vol. 153, no. 5, pp. 726-734, Sept 2006.

[18] E.M.Schulz and R.E.Betz, "Optimal torque per amp for brushless doubly fed reluctance machines," *Proc. of IEEE IAS Annual Meeting,* vol. 3, pp. 1749-1753, Hong Kong, October 2005.

[19] M.G.Jovanovic, J.Yu, and E.Levi, "Direct torque control of brushless doubly fed reluctance machines," *Electric Power Components and Systems,* vol. 32, no. 10, pp. 941-958, October 2004.

[20] M.G.Jovanovic, J.Yu, and E.Levi, "Encoderless direct torque controller for limited speed range applications of brushless doubly fed reluctance motors," *IEEE Transactions on Industry Applications,* vol. 42, no. 3, pp. 712-722, May/June 2006.

[21] Y Liao and C. Sun, "A novel position sensorless control scheme for doubly fed reluctance motor drives," *IEEE Trans. on Industry Applications,* vol. 30, no. 5, pp. 1210-1218, Sept/Oct 1994.

[22] M.G.Jovanovic, J.Yu, and E.Levi, "A doubly-fed reluctance motor drive with sensorless direct torque control," *Proc. of IEEE International Electric Machines and Drives Conference (IEMDC),* vol. 3, pp. 1518-1524, Madison, Wisconsin, June 2003.

[23] F. Liang, L. Xu, and T. Lipo, "D-q analysis of a variable speed doubly AC excited reluctance motor," *Electric Machines and Power Systems,* vol. 19, no. 2, pp. 125-138, March 1991.

[24] I.Takahashi and T.Noguchi, "A new quick-response and high-efficiency control strategy of an induction machine," *IEEE Transactions on Industry Applications,* vol. IA-22, no. 5, pp. 820-827, Sept/Oct 1986.

[25] I.Takahashi and Y.Ohmori, "High performance direct torque control of an induction motor," *IEEE Transactions on Industry Applications,* vol. 25, no. 2, pp. 257-264, Mar/Apr 1989.

[26] W.R.Brassfield, R.Spee, and T.G.Habetler, "Direct torque control for brushless doubly-fed machines," *IEEE Transactions on Industry Applications,* vol. 32, no. 5, pp. 1098-1104, 1996.

[27] S.Arnalte, J.C.Burgos, and J.L.Rodriguez-Amenedo, "Direct torque control of a doubly-fed induction generator for variable speed wind turbines," *Electric power components and systems,* vol. 30, pp. 199-216, 2002.

[28] L. Xu and P. Cartwright, "Direct active and reactive power control of DFIG for wind energy generation," *IEEE Transactions on Energy Conversion,* vol. 21, no. 3, pp. 750-758, September 2006.

[29] D. Zhi and L. Xu, "Direct power control of DFIG with constant switching frequency and improved transient performance," *IEEE Transactions on Energy Conversion,* vol. 22, no. 1, pp. 110—118, March 2007.

[30] G. Abad, M. A. Rodriguez, and J. Poza, "Two-level VSC-based predictive direct torque control of the doubly fed induction machine with reduced power ripple at low constant switching frequency," *IEEE Transactions on Energy Conversion,* vol. 23, no. 2, pp. 570-580, June 2008.

[31] "Three-level NPC converter-based predictive direct power control of the doubly fed induction machine at low constant switching frequency," *IEEE Transactions on Industrial Electronics,* vol. 55, no. 12, pp. 4417–4429, December 2008.

[32] "Two-level VSC based predictive direct torque control ofthe doubly fed induction machine with reduced torque and flux ripples at low constant switching frequency," *IEEE Transactions on Power Electronics,* vol. 23, no. 3, pp. 1050-1061, May 2008.

[33] R. Datta and V.T.Ranganathan, "Direct power control of grid-connected wound rotor induction machine without rotor position sensors," *IEEE Transactions on Power Electronics,* vol. 16, no. 3, pp. 390-399, May 2001.